Hindawi Publishing Corporation
Advances in Materials Science and Engineering
Volume 2014, Article ID 101872, 9 pages
http://dx.doi.org/10.1155/2014/101872

Research Article

Effect of Casting Parameters on the Microstructural and Mechanical Behavior of Magnesium AZ31-B Alloy Strips Cast on a Single Belt Casting Simulator

Ahmad Changizi,[1,2] Mamoun Medraj,[1] and Mihaiela Isac[2]

[1] *Mechanical and Industrial Engineering Department, Concordia University, Sir George Williams Campus, 1515 St. Catherine W., Montreal, QC, Canada H3G 2W1*
[2] *McGill Metal Processing Center, McGill University, 3610 University Street, Montreal, QC, Canada H3A 2B2*

Correspondence should be addressed to Ahmad Changizi; ah_chang@alumni.concordia.ca

Received 21 May 2013; Revised 1 October 2013; Accepted 21 October 2013; Published 19 January 2014

Academic Editor: Aloysius Soon

Strips of magnesium alloy AZ31-B were cast on a simulator of a horizontal single belt caster incorporating a moving mold system. Mixtures of CO_2 and sulfur hexafluoride (SF_6) gases were used as protective atmosphere during melting and casting. The castability of the AZ31-B strips was investigated for a smooth, low carbon steel substrate, and six copper substrates with various textures and roughnesses. Graphite powder was used to coat the substrates. The correlation between strip thickness and heat flux was investigated. It was found that the heat flux from the forming strip to the copper substrate was higher than that to the steel substrate, while coated substrates registered lower heat fluxes than uncoated substrates. The highest heat flux from the strip was recorded for casting on macrotextured copper substrates with 0.15 mm grooves. As the thickness of the strip decreased, the net heat flux decreased. As the heat flux increased, the grain sizes of the strips were reduced, and the SDAS decreased. The mechanical properties were improved when the heat flux increased. The black layers which formed on the strips' surfaces were analyzed and identified as nanoscale MgO particles. Nano-Scale particles act as light traps and appeared black.

1. Introduction

Magnesium is the lightest structural metal in common use [1]. Similarly, supplies of magnesium ores are virtually inexhaustible. Magnesium alloys normally have very good castability and machinability, as well as excellent specific strength and stiffness [2]. However magnesium alloys have some difficulty during rolling due to hexagonal close packed (hcp) lattice structure [3]. Meanwhile, a fine grain structure increases strength and ductility by promoting the operation of nonbasal slip systems and limiting twinning in magnesium alloys [4]. Strip casting of magnesium has become important in recent years. For reducing the cost of thin sheets of magnesium alloys, strip casting technologies such as horizontal single belt casting (HSBC), twin roll casting (TRC), and twin belt casting (TBC) have been developed [3]. With a strip casting process, magnesium alloy strips can typically be produced in thicknesses of 1–10 mm [1]. Direct strip casting, or HSBC, as a near-net-shape casting process, has potential use in the processing of aluminum, copper, zinc, and lead alloys, directly into sheet products.

Generally, most metals and alloys are amenable to direct casting into plates, strips, or ribbons. However, a metallurgical understanding of these materials is needed to determine their suitability for casting into thin-gauge strips. Technically, the evaluation of a process must take into account the melting point of the alloy, the freezing range, the oxidation resistance in both the liquid and solid states, the heat transfer behavior, the fluidity of the melt, and the number and type of the liquid-to-solid, and solid-state, transformations that may occur. There is a particular emphasis on magnesium alloys as these are the major candidates for large-scale production by this processing route, given the poor hot rolling capabilities caused by its hexagonal close packed structure [5, 6]. The present study was carried out to investigate the possibility of directly casting magnesium strip products on a horizontal

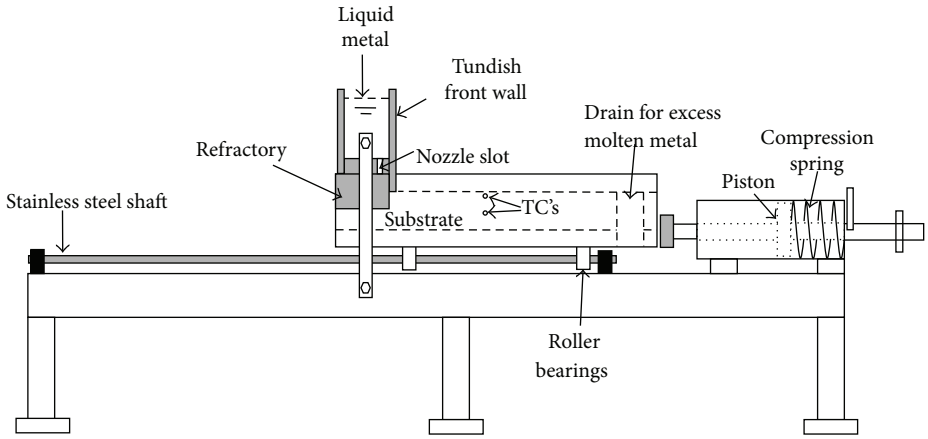

Figure 1: Schematic of the strip casting single belt simulator.

single belt caster (HSBC). The alloy studied was the AZ31-B magnesium alloy.

2. Experimental Procedure

2.1. Raw Materials and Melting Unit. Commercial magnesium alloy AZ31 grade B bar ingots obtained from Magnesium Electron Co. were used as raw material in the present experiments. The raw bar ingot materials were cut into smaller pieces and prepared for melting. Graphite powder, comprising particles of 0.5–0.6 μm, obtained from Asbury Carbons Co., was used to coat the casting substrates. The graphite was of a synthetic variety, and the particles in general were flake shaped.

2.2. Strip Casting Simulator. A schematic overview of the strip casting simulator is shown in Figure 1. The equipment includes the following: a containment mould, a substrate onto which the melt can be poured, a tundish, a motor that drags the substrate at preselected casting speeds, and a data acquisition system. The simulator can be set to produce strips of $w(80) \times l(1100) \times t(1 - 5)$ mm dimensions. The casting substrates can be coated with different materials such as the graphite used in the present research. In order to measure local heat fluxes, two K type thermocouples were placed in each segment of the substrate; one was set near the surface and the other was placed slightly below the first thermocouple.

2.3. Substrate Specification. Two types of material substrates were used in the present experiments, steel with a polished surface and pure copper with six differently textured inserts/segments. Figure 2 illustrates the schematics along with photos of the six copper substrates (2 × 2 inch segments). Table 1 provides dimensional specifications of different areas of copper chill substrate. Each segment had a different macrotexture.

2.4. Melting and Pouring of Molten Metal. The melt was prepared in a closed steel crucible, in which the atmosphere of the melt was protected from air ingress at all steps in the casting process, so as to avoid any oxidation or possible burning. The protective atmosphere comprised a mixture

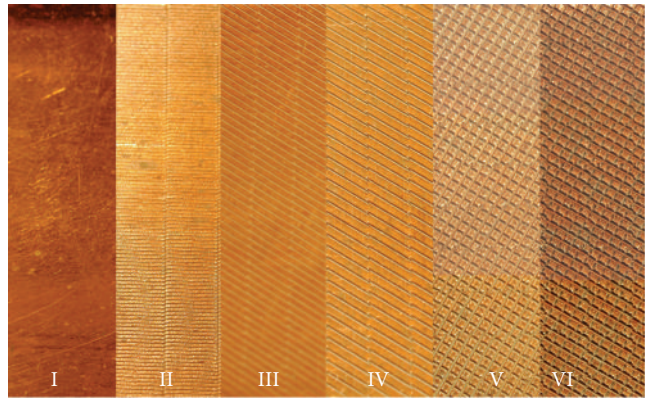

Figure 2: Schematic and photos of different areas of copper substrate.

Table 1: Dimensional specifications of different areas of copper substrate presented in Figure 2.

Segment	a (μm)	x (μm)	y (μm)	z (mm)
I	0	0	0	0
II	64.4	477.7	90	7
III	78.5	825	150	8
IV	317	1103	240	320
V	488	998	300	0.99
VI	451	1074	600	1.07

of sulfur hexafluoride, 0.5% SF_6, in a carrier gas of carbon dioxide, 99.5% CO_2.

The molten metal was heated using an induction furnace, to a temperature of 710°C, which is above the pouring temperature, 700°C, in order to provide sufficient superheat for skimming and metal transferring purposes. The molten metal was poured directly from the crucible into the tundish to avoid any large temperature drops. Before pouring, the tundish was preheated up to 150°C for drying the refractory walls inside the tundish. At the same time, the substrate was preheated to 30°C for avoiding any moisture. Transferring and pouring the molten metal were done manually. The substrate was propelled by a loaded spring at a constant speed of 0.5 m/sec.

2.5. Calculating Heat Flux and Applying IHCP to a Horizontal Single Belt Casting Simulator. Beck put forward a nonlinear estimation method to deal with phase changes and temperature dependent thermal properties of the solidification process used for solving the IHCP [9]. To treat experimental data, statistical principles and the concept of amplitudes temperatures are applied to the thermal capacity and heat conduction of the substrate during subsurface temperature measurements. This application is performed using a nonlinear estimation method to solve the delayed and diminished thermal response problems. The heat flux is taken to be a constant or a linear function of time within a given time interval. This is the principle of Beck's nonlinear estimation technique, according to which the heat flux is then determined for that period according to the following function:

$$F(q) = \sum_{i}^{N_1} \sum_{j}^{N_2(N_3+1)} \left(T_{ij} - Y_{ij}\right)^2, \quad (1)$$

where N_1 is the number of internal points in the temperature measurement excluding those used for boundary condition. N_2 is the number of temperature measurements per time interval. N_3 is the future number of time intervals considered for the heat flux calculation at each time interval. T_{ij} and Y_{ij} are the calculated and measured temperatures of location i and the time instant j, respectively [10].

The IHCP (Inverse Heat Conduction Problem) applied for the interface between the melt and substrate is shown schematically in Figure 3; the bounding conditions for the governing differential equation (2) are expressed in (3), (4), and (5) [11] as follows:

$$\rho C_p \left(\frac{\partial T}{\partial t}\right) = k \frac{\partial^2 T}{\partial x^2}, \quad (2)$$

$$-k \frac{\partial T}{\partial t}\Big|_{x=0} = q_1 \quad t > t_{l-1}, \quad (3)$$

$$T\left(x_1, t = t_{l-1}\right) = F\left(x_1\right), \quad (4)$$

$$T\left(x_2, t = t_{l-1}\right) = F\left(x_2\right). \quad (5)$$

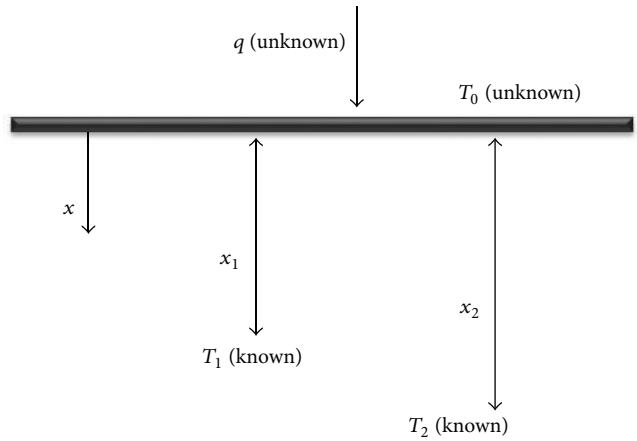

Figure 3: Schematic of applying IHCP to deduce interfacial heat fluxes for the single belt strip casting simulator.

The corresponding differential equation and boundary conditions for sensitivity coefficients are [2]

$$\rho C_p \frac{\partial \text{Ø}}{\partial t} = k \frac{\partial^2 \text{Ø}}{\partial x^2},$$

$$-k \frac{\partial \text{Ø}}{\partial x}\Big|_{x=0} = 1 \quad 1 > t_{l-1},$$

$$\text{Ø}\left(x_1, t = t_{l-1}\right) = 0,$$

$$\text{Ø}\left(x_2, t = t_{l-1}\right) = 0, \quad (6)$$

where Ø is a sensitivity coefficient and subscript i denotes the time when it was applied. In this investigation, temperatures are recorded using two thermocouples for each segment of the substrate connected to an Omega Data Acquisition System. In order to convert the time versus temperature data to time versus heat flux, the necessary IHCP software was developed from first principles by Isac et al. [7].

3. Results and Discussion

3.1. Effect of Substrate Material on Heat Flux. Materials of the substrate in the strip casting process are one of the important issues which affect casting parameters. Table 2 shows the values of the maximum heat fluxes recorded for different substrate materials. The casting conditions (speed, superheat, and thickness) were the same.

The thermophysical properties of different substrate materials used in the present experiments are summarized in Table 3.

The measured interfacial heat flux is related to the thermal conductivity and thermal diffusivity of the substrate. Hence, the large difference between the thermal conductivity, k, of steel and copper is reflected in the value of the heat flux at the mould/melt interface. The bare copper substrate with no graphite coating had the highest cooling capacity and produced the highest heat flux at the mould/melt interface. Because of the poor thermal conductivity of graphite and of

Table 2: Value of maximum heat flux for different substrate materials.

Substrate materials	Coating	R_a	Max. heat flux MW/m^2
Steel	No	0	1.29
Copper	No	0	5.06
Steel	Yes	0	0.71
Copper	Yes	0	2.85

Table 3: Thermophysical properties of the substrates used [7, 8].

Substrate materials	C_p (kJ/kg °C)	k (W/m·K)	ρ (kg/m^3)	α (cm^2/sec)
Carbon steel	0.486	48	7753	0.081
Copper	0.383	386	8954	0.415
Graphite	0.71	24	2200	0.0024

steel, the steel substrate coated with a graphite layer had the smallest heat flux at the mould/melt interface.

3.2. Effect of the Surface Topography of the Substrate on the Interfacial Heat Flux. In the HSBC casting procedure, the metal/mould interface is not in perfect thermal contact. Localized heat flows through the actual contact points between the metal/mould interfaces are significantly less than in the case of perfect contact.

Consider the melt hanging between two parallel running peaks at a distance of 2λ apart; then the melt sag (d_{sag}) depends on the melt surface tension (σ) and the metallostatic pressure (ΔP) for a nonwetting substrate. The radius of the metal curvature, R, is [12]

$$R = \frac{\sigma}{\Delta P} = \frac{\sigma}{\rho g h}, \tag{7}$$

where σ is the melt surface tension, ρ is the melt density, g is the gravitational constant, and h is the melt height. The melt sag can be calculated as [5, 13]

$$d_{sag} = R - \sqrt{R^2 - \lambda^2}. \tag{8}$$

However significant thermal resistance exists at the substrate/melt interface because of trapped air, oxide layers, gaps made by shrinkage of the solidifying shell from the interface, thermal expansion of the mold, and so forth.

Table 4 presents the results of measured heat fluxes for different surface topographies. The maximum heat fluxes were measured in segment III, for both coated and uncoated substrates, while minimum heat fluxes were measured in segment VI. We can conclude that the substrate topography of segment number six had an increased thermal resistance compared to that of segment number three.

Consequently, the maximum surface contact of melt-mould occurred with segment III and the highest number of air pockets was in segment VI.

3.3. Effect of Coating of Substrates on Measured Heat Fluxes. Figure 4 illustrates the measured heat fluxes of casting strips of magnesium AZ31-B alloy on substrates with various roughnesses, with and without a graphite coating. The measured heat fluxes on graphite-coated substrates were all lower than those on equivalent (matching) bare substrates.

Table 4: Maximum values of heat flux from 3 mm strips of magnesium cast on macrotextured copper substrate.

Segment no.	Coating	Depth of grooves (mm)	Max. heat flux (MW/m^2)
I	No	0	5.06
II	No	0.09	5.78
III	No	0.15	6.60
IV	No	0.24	5.18
V	No	0.3	4.38
VI	No	0.6	3.35
I	Yes	0	2.85
II	Yes	0.09	3.20
III	Yes	0.15	3.53
IV	Yes	0.24	2.93
V	Yes	0.3	2.58
VI	Yes	0.6	2.50

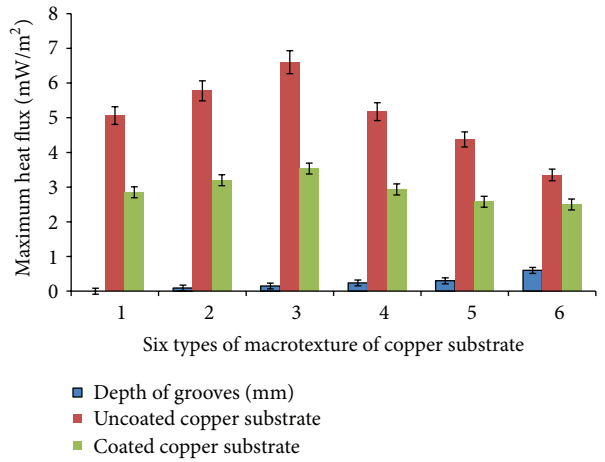

Figure 4: Effect of surface topology of substrate on heat flux with and without coating.

3.4. Effect of Strip Thickness on Heat Flux. The distance between the nozzle and the substrate was decreased, so as to reduce the thickness of the strips produced from 3 to 1 mm. The substrate was coated with a layer of fine graphite to a thickness of 60 μm. Based on Figure 5 and the following equations, it is evident that if one increases the strip thickness, the amount of heat transferred from the strip to the substrate must increase. Essentially, the total amount of the heat loss per unit area required to complete solidification of the liquid metal is

$$\Delta Q_t = \rho \cdot d \left\{ C_p \left(T_c - T_M \right) + \Delta H \right\}, \tag{9}$$

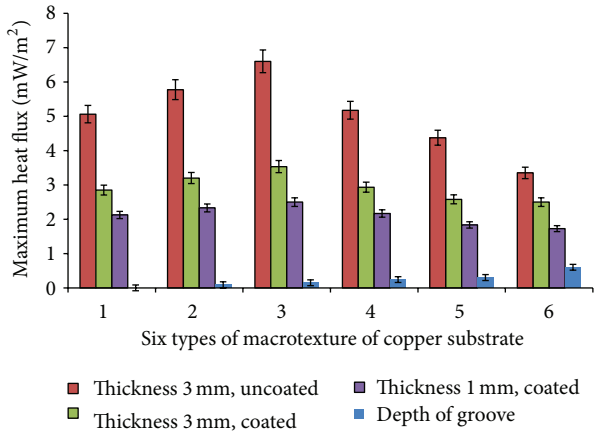

Figure 5: Heat flux versus strip thickness and substrate textures.

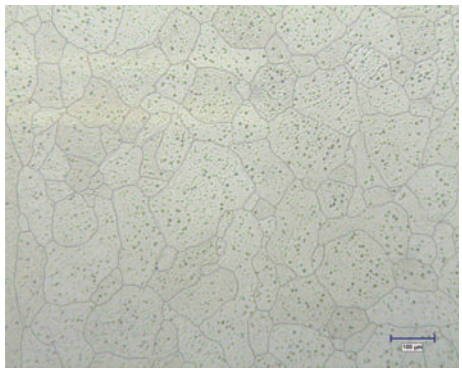

Figure 6: Microstructure of top surface of AZ31-B strip cast on segment III of copper substrate without any graphite coating.

where ρ is the density of liquid metal, d is the thickness of strip produced, C_p is the specific heat, T_c is the casting temperature, T_M is the melting point, and ΔH is the latent heat of fusion/mass. Note that $\rho \cdot d\{C_p(T_c - T_M)\}$ is the sensible heat of the melt and $\rho \cdot d \cdot \Delta H$ is the latent heat component.

3.5. Microstructural Analysis. Figure 6 shows a microstructure of AZ31-B magnesium alloy close to the strips top surface when casting 3 mm strip on segment III of the copper substrate without any graphite coating.

It has been claimed by Rappaz and Gandin [13] that the dendrites developed at the interface with the substrate were not inclined, their growth direction being verticality upwards given that the direction of the fluid flow directly influences the growth direction of dendrites at the melt/substrate interface. The dendritic growth mechanism in magnesium AZ31-B alloys has been elaborated by Vander [14]. It is concluded that a similar principle governs the dendritic growth for magnesium AZ31-B alloy investigated in this work. During the solidification of the alloy, a symmetrical solute field at the dendrite tip is established. Accordingly, the solute gradient is uniform on both sides of the dendrite tip during the growth. Thus the main origin of the dendrite growth direction is deemed to be the solute distribution. According to the literature [15, 16], the nonhomogeneous distribution of solute atoms between dendrite arms in a magnesium AZ31-B alloy is mainly due to the fact that the solidification takes place over a range of temperatures. In fact, there is insufficient time for atomic diffusion to redistribute the solute both within the liquid in the vicinity of the solid-liquid interface and within the solid, since cooling occurs so rapidly through the two-phase (L + S) regime. By comparing the microstructures of the bottom surfaces of strips, it can be concluded that the grain size depends significantly on the heat flux. The results of microstructural analyses of all samples are summarized in Table 5.

As shown in Table 5, with decreasing heat flux and increasing thermal resistance between the substrate and the strip, the grain size increases. The grain size of the top surface is larger than that of the bottom surface because of solidification delay due to smaller heat fluxes at the top surface. Secondary dendrite arm spacing (SDAS) is found to be directly related to heat flux and thermal contact resistance. The SDAS decreases when air pockets are generally trapped at the substrate/melt interface, which dramatically reduces the heat flux, as explained earlier. The occurrence of these air pockets can subsequently influence the microstructure of the strips. Consequently, the grains tend to grow up from the bottom surface to the top surface resulting in a columnar pattern of grain growth. The effect of these air pockets on the grain structure is clearly shown in Figure 7. A similar observation pertaining to the effect of air pocket formation on the strip's microstructure has been reported by Dubé et al. [17].

3.6. Phase Analysis. Scanning Electron Microscopy was used to analyze the chemistry and morphology of the secondary phases present in the strip microstructure, as shown in Figure 8.

The microanalyses using EDX technique, were performed on the intermetallics marked in Figure 8, in order to identify their composition. Figure 9 presents one X-Ray spectrum of the analyzed intermetallics.

EDX analysis, demonstrated in the associated spectra, indicates that the phases contain Mg, Zn, Al, and Mn. The presence of magnesium in the spectra could originate from either the matrix or the intermetallics. Based on the information from the phase diagram, the matrix is α-Mg, and the particles are Mg-Al-Zn phase (most likely $(Al,Zn)_{49}Mg_{32}$) and Al-Mn (it could be a mixture of $Al_{11}Mn_4$, Al_8Mn_5, Al_9Mn_{11}, and β-Mn(Al)) intermetallics. However, according to the investigation by Cao et al. [18], the α-Mg is a solid solution of Mg-Al-Zn-Mn.

3.7. Analysis of Mechanical Properties of AZ31-B Strips. Figure 10 and Table 6 summarize the mechanical properties of the strip cast AZ31-B strips. The tensile and yield strength are calculated using equations TS (MPa) = 3.4 × BHN and $H = 3\sigma_y$. Local Vickers hardness was taken on the cross section of the strips. There was no significant difference between hardness values taken at the top and the bottom surfaces of the strips.

Table 5: Microstructure analyses of strips.

Depth of groove	Thickness	Coating	Heat flux	Grain Size (μm)		SDAS (μm)	
				Bottom	Top	Bottom	Top
0.15	3 mm	No	6.6	35	100	5.39	6.1
0.09	3 mm	No	5.775	64	110	7.7	6.14
0.24	3 mm	No	5.175	70	117	8.5	7.15
0	3 mm	No	5.062	77	121	8.6	9.2
0.3	3 mm	No	4.375	91	136	8.9	10
0.6	3 mm	No	3.35	92	138	9.02	10.5
0.15	3 mm	Yes	3.5	103	110	8.5	9.1
0.09	3 mm	Yes	3.2	108	120	10.04	11.8
0.24	3 mm	Yes	2.9	110	127	10.8	12.4
0	3 mm	Yes	2.85	115	129	11.5	12.8
0.3	3 mm	Yes	2.58	132	137	11.58	13.5
0.6	3 mm	Yes	2.5	134	140	11.91	13.8
0.15	1 mm	Yes	2.5	108	132	8.2	9.8
0.09	1 mm	Yes	2.33	125	135	10.5	11
0.24	1 mm	Yes	2.166	138	142	11.7	12.4
0	1 mm	Yes	2.12	140	150	12.2	14
0.3	1 mm	Yes	1.83	150	162	12.4	15.6
0.6	1 mm	Yes	1.72	155	175	13	17
0 (steel)	3 mm	No	1.2	157	225	14	18
		Yes	0.71	350	470	20	25

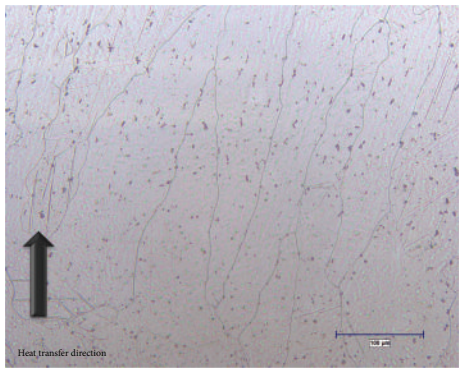

Figure 7: Directional grain growth because of air pockets at the melt/mould interface, ×200.

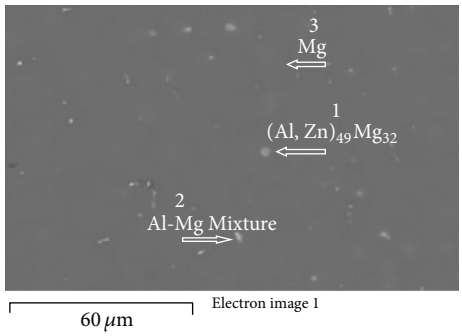

Figure 8: SEM image of AZ31-B strip.

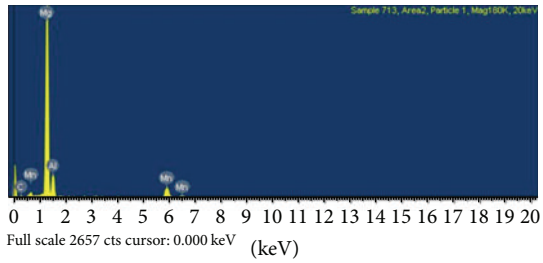

Figure 9: EDX analyses of point 2 of Figure 8.

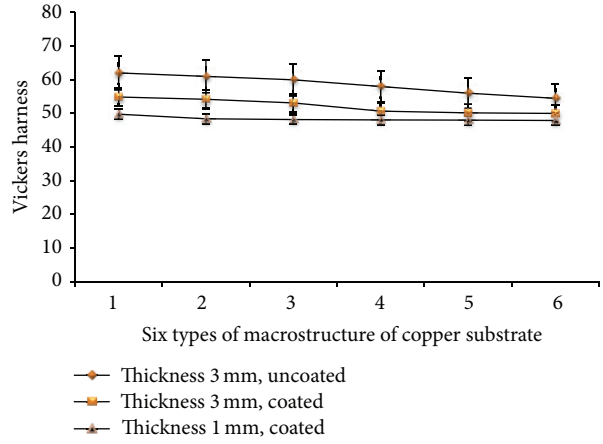

Figure 10: The effect of heat flux on the hardness of AZ31-B strips.

Table 6: Mechanical properties of AZ31-B strips.

Substrate no.	Depth of groove (mm)	Thickness	Coating	Heat flux	R_c $W/m^2\,^\circ C \times 10^{-4}$	HV	YS MPa	TS MPa
III (c)	0.15	3 mm	No	6.6	4.545	62	147	166.6
II (b)	0.09	3 mm	No	5.77	5.195	61	144	163.2
IV (d)	0.24	3 mm	No	5.17	5.797	60	144	163.2
I (a)	0	3 mm	No	5.06	5.927	58	141	159.8
V (e)	0.3	3 mm	No	4.37	6.857	56	138	156.4
VI (f)	0.6	3 mm	No	3.35	8.955	54.5	135	153
III (c)	0.15	3 mm	Yes	3.5	8.571	54.9	135	153
II (b)	0.09	3 mm	Yes	3.2	9.375	54.2	135	153
IV (d)	0.24	3 mm	Yes	2.9	10.345	53.1	132	149.6
I (a)	0	3 mm	Yes	2.85	10.526	50.7	141	159.8
V (e)	0.3	3 mm	Yes	2.5	11.628	50.2	141	159.8
VI (f)	0.6	3 mm	Yes	2.5	12.000	50	141	159.8
III (c)	0.15	1 mm	Yes	2.5	4.000	49.8	126	142.8
II (b)	0.09	1 mm	Yes	2.33	4.292	48.4	126	142.8
IV (d)	0.24	1 mm	Yes	2.16	4.617	48.2	126	142.8
I (a)	0	1 mm	Yes	2.12	4.717	48.1	126	142.8
V (e)	0.3	1 mm	Yes	1.83	5.464	48	126	142.8
VI (f)	0.6	1 mm	Yes	1.72	5.814	47.9	123	139.4
I	0 (steel)	3 mm	No	1.2	25.000	47.5	123	139.4
			Yes	0.71	42.254	47	123	139.4

Figure 11: Black layer of coating on strip cast without protective atmosphere.

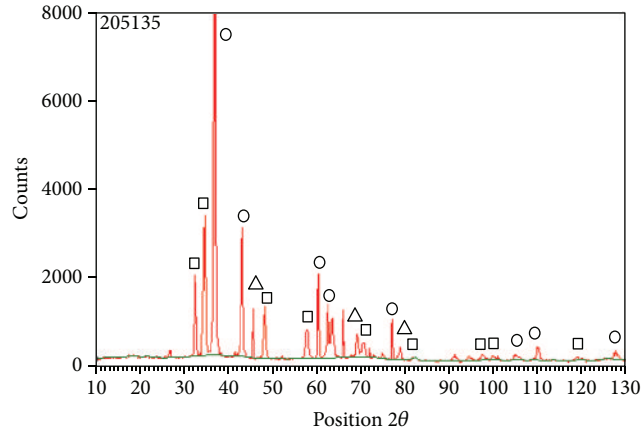

Figure 12: XRD pattern of black layer.

Based on the experimental results presented above, as the heat flux increases, the hardness and the other mechanical properties increased. In the case of 1 mm thick strip, because of lower weight pressure of the strip on the substrate, the thickness of the air gap between the strip and substrate was increased, and the heat transfer rate from strip to substrate decreased. Based on the lower global heat fluxes, represented as the area under the heat flux-time curve, in strips with 1 mm thickness, grain sizes were large and mechanical properties were lower. This issue was presented in detail in Section 3.5.

3.8. Evaluation of the Black Layer on AZ31-B Strip Surface When Cast in Air. To protect magnesium alloys from oxidation during strip casting, a mixture of CO_2 and SF_6 is usually used. If not, a black layer film on the surface of the strip forms as shown in Figure 11. This layer is strongly adherent, and severely compromises the surface quality of the strip for commercial proposes.

XRD tests were performed in order to analyze the nature of the black layer, as shown in Figure 12.

Figures 13(a) and 13(b), respectively, present an SEM image and an EDX spectrum of the black layer formed on the strip surface when cast in air.

It is well known that, under normal conditions, MgO is white and $MgAl_2O_4$ is colorless. According to XRD and EDX

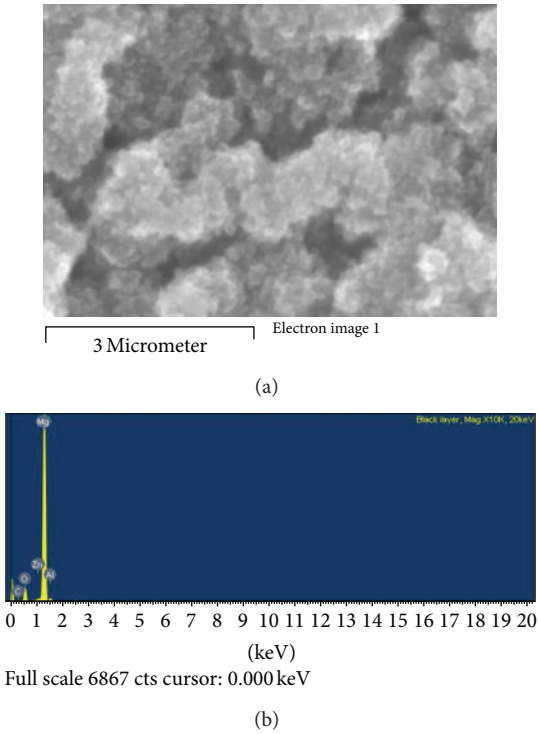

Figure 13: (a) SEM image of the black layer. (b) EDX analysis of the black layer.

patterns, the major component of the layer on the strip is definitely MgO. As shown in the SEM image, the particle sizes of MgO are around 0.1 μm. According to the literature [19–22], if the particle size of the oxide is so small that it acts as a light trap, then it will appear black. It should be noted that Mg peaks in the XRD and EDX patterns emanated from the base metal, not from the thin black layer of MgO particles forming on top of the cast strip. Clearly, it will be necessary to use a protective atmosphere in the commercial strip casting of magnesium alloys.

4. Conclusions

In the present research, the effects of casting parameters on the properties of strips of AZ31-B alloy have been investigated. The effect of heat flux on the microstructure and mechanical properties were studied as well. The following conclusions can be drawn.

(1) As substrate roughness increased beyond 0.15 mm for macroscopically grooved substrates, the thermal resistance increased, while heat fluxes decreased.

(2) As the thickness of strip increased, the heat flux into the substrates increased.

(3) As the interfacial heat flux increased, the grain size and the SDAS across the strip were decreased.

(4) No significant differences were recorded between hardness values taken at the top and the bottom surfaces of the strips.

(5) As heat fluxes increased and the grain sizes decreased, mechanical properties, TS, YS, and HV, all increased.

(6) Microstructural analyses of AZ31-B strips revealed that the finest grain sizes and lowest SDAS were obtained using a copper substrate versus a steel substrate.

(7) Coated substrates reduced the capability of heat extraction but stabilized the dimensions of strip and gave a good surface quality.

(8) The black layer on the strips cast in air is composed of small particles of MgO (in the 100 nm range).

Conflict of Interests

The authors declare that there is no conflict of interests regarding the publication of this paper.

References

[1] G.-S. Wang, H.-S. Di, and F. Huang, "Preparation of AZ31 magnesium alloy strips using vertical twin-roll caster," *Transactions of Nonferrous Metals Society of China*, vol. 20, no. 6, pp. 973–979, 2010.

[2] J. Kim, *Interfacial heat transfer of a single belt casting process [M.S. thesis]*, McGill University, Montreal, Canada, 2002.

[3] A. Zi and H. Palkowski, "Direct strip casting and hot rolling of an AZ31 magnesium alloy," *Materials Science and Engineering A*, vol. 528, no. 2, pp. 559–565, 2010.

[4] S. Das, S. Ji, O. El Fakir et al., "Melt conditioned twin roll casting (MC-TRC) of thin Mg-Alloy strips for direct stamping of Mg components," *Materials Science Forum*, vol. 765, pp. 170–174, 2013.

[5] D. Li, L. E. Calzado, M. Isac, and R. Guthrie, "Improving the surface of AA6111 sheet material, cast at high speeds, through the use of macroscopically textured substrates," in *Proceedings of the TMS Annual Meeting and Exhibition (Light Metals '09)*, pp. 889–894, San Francisco, Calif, USA, February 2009.

[6] J. S. Kim, M. Isac, and R. I. L. Guthrie, "Metal-mold heat transfer and solidification of magnesium alloys in belt casting processes," in *Proceedings of the Magnesium Technology (TMS '04)*, pp. 247–257, Charlotte, NC, USA, 2004.

[7] M. Isac, R. Tavares, P. Netto, and R. I. L. Guthrie, "The influence of coated mould on heat transfer and microstructure for horizontal strip casting of aluminium alloys," in *Proceedings of the 15th International Thermal Spray Conference*, pp. 1025–1032, Nice, France, May 1998.

[8] M. Warren, J. Rohsenow, Y. Hartnett, and C. Cho, *Handbook of Heat Transfer*, McGraw Hill, New York, NY, USA, 1998.

[9] J. V. Beck, "Nonlinear estimation applied to the nonlinear inverse heat conduction problem," *International Journal of Heat and Mass Transfer*, vol. 13, no. 4, pp. 703–716, 1970.

[10] J. Kim, *Interfacial heat transfer and solidification of Mg and Al alloys in single belt casting process [Ph.D. thesis]*, McGill University, Montreal, Canada, 2006.

[11] J. S. Kim, M. Isac, R. I. L. Guthrie, and J. Byun, "Studies of interfacial heat transfer resistances and characterization of strip microstructures for Al-Mg alloys cast on a single belt casting simulator," *Canadian Metallurgical Quarterly*, vol. 41, no. 1, pp. 87–96, 2002.

[12] L. Strezov and J. Herbertson, "Experimental studies of interfacial heat transfer and initial solidification pertinent to strip casting," *ISIJ International*, vol. 38, no. 9, pp. 959–966, 1998.

[13] M. Rappaz and C.-A. Gandin, "Probabilistic modelling of microstructure formation in solidification processes," *Acta Metallurgica et Materialia*, vol. 41, no. 2, pp. 345–360, 1993.

[14] F. Vander, *Metallography and Microstructures*, vol. 9, ASM International, Materials Park, Ohio, USA, 1994.

[15] M. Ferry, *Direct Strip Casting of Metals and Alloys*, Woodhead Publication in Materials, Cambridge, UK, 2006.

[16] J. T. Wang, M. X. Liang, Q. Kuang, M. Gurvan, G. Chen, and K. Xia, "Microstructure and mechanical properties of alloy AZ31 after equal channel angular pressing," *Materials Forum*, vol. 29, no. 2, pp. 370–375, 2005.

[17] D. Dubé, A. Couture, Y. Carbonneau, M. Fiset, R. Angers, and R. Tremblay, "Secondary dendrite arm spacings in magnesium alloy AZ91D: from plaster moulding to laser remelting," *International Journal of Cast Metals Research*, vol. 11, no. 3, pp. 139–144, 1998.

[18] P. Cao, D. H. StJohn, and M. Qian, "The effect of manganese on the grain size of commercial AZ31 alloy," *Materials Science Forum*, vol. 488-489, pp. 139–142, 2005.

[19] S. I. Berman, V. I. Zalesskii, K. I. Imanov, and V. A. Shelamov, "Effect of the degree of deformation on the mechanical properties and structure of extruded semifinished products from granules of aluminum alloys of the system Al-Zn-Mg-Cu," *Soviet Powder Metallurgy and Metal Ceramics*, vol. 8, no. 12, pp. 966–969, 1969.

[20] I. K. Ludlow, "Symmetry of a colour centre in magnesium oxide," *Proceedings of the Physical Society*, vol. 88, no. 3, article 323, pp. 763–770, 1966.

[21] M. A. Shand, *The Chemistry and Technology of Magnesia*, John Wiley & Sons, New York, NY, USA, 2006.

[22] B. Haxby, *A study of color centers in magnesium-oxide [Ph.D. thesis]*, University of Minnesota, Minneapolis, Minn, USA, 1957.